Contrasting distribution of REE and yttrium among particulate, colloidal and dissolved fractions during low and high flows in peri-urban and agricultural river systems

Loïc A Martin, Davide A.L. Vignati, Christophe Hissler

Science of the Total Environment 790 (2021) 148207

Contents lists available at ScienceDirect

Science of the Total Environment

journal homepage: www.elsevier.com/locate/scitotenv

Contrasting distribution of REE and yttrium among particulate, colloidal and dissolved fractions during low and high flows in peri-urban and agricultural river systems

Loïc A. Martin [a], Davide A.L. Vignati [b], Christophe Hissler [a,*]

[a] CAT/ENVISION/ERIN Research Group, Luxembourg Institute of Science and Technology, Belvaux, Luxembourg
[b] Université de Lorraine, CNRS, LIEC, F-57000 Metz, France

HIGHLIGHTS

- REY particulate fraction results from soil erosion in all hydrological conditions.
- Dissolved REY fraction reflects WWTP effluent during low flow.
- Anthropogenic REY are observed in all fractions except small colloids.
- Dilution and natural inputs hide REY anthropogenic anomalies during high flow.
- Observed Eu anomaly could be due to Gd transmetallation during WWTP process.

GRAPHICAL ABSTRACT

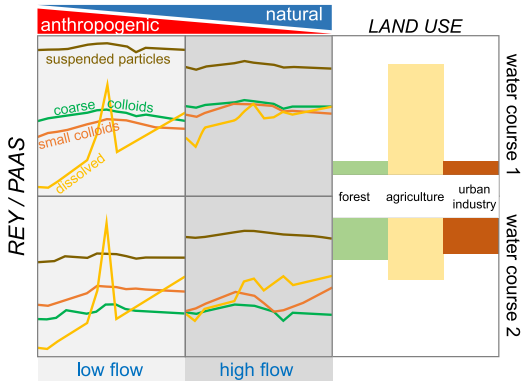

ARTICLE INFO

Article history:
Received 27 January 2021
Received in revised form 26 May 2021
Accepted 30 May 2021
Available online 2 June 2021

Editor: José Virgílio Cruz

Keywords:
Elemental partitioning
Rare earth elements
Methodological error
Human activities
Hydrological conditions
Alzette River
Luxembourg

ABSTRACT

Understanding the possible consequences of anthropogenic activities on REY environmental fate and adverse effects on biota requires a detailed knowledge of their distribution between the particulate, colloidal and dissolved fractions. Such information is practically non-existent for peri-urban rivers having heavily populated basins and suffering from direct impacts from various human activities. The present study compared the distribution of REY among the particulate (>1000 nm), coarse colloidal (1000 nm – 220 nm), small colloidal (220 nm – 10 kDa) and dissolved (<10 kDa) water fractions in two peri-urban river basins having contrasted land uses (agricultural vs urban/industrial) under low and high flow conditions. Regardless of hydrological conditions, most of the REY were in the particulate fraction for both catchments. These results suggest erosion of soils as the main source of particulate REY in the two rivers, although a Nd anomaly of industrial origin occurred in the particulate and coarse colloidal fractions of the industrialized river basin. During low flow, the REY patterns of the dissolved fraction displayed marked Gd and Eu anomalies and a fractionation between Light REY and Heavy REY. Both characteristics reflect the influence of wastewater treatment plant effluents on the dissolved REY patterns in the two rivers. During high flow, the dissolved fraction acquired a less fractionated, more natural Light REY and Middle REY pattern, including much lower Gd and Eu positive anomalies. The REY fractionation of the coarse colloidal fraction was close to the particulate, while small colloids were depleted in Light REY and more similar to the dissolved fraction. These different patterns suggest a difference in the nature of REY bearing phases between the two

* Corresponding author.
E-mail address: christophe.hissler@list.lu (C. Hissler).

https://doi.org/10.1016/j.scitotenv.2021.148207

colloidal fractions. The available results collectively show that a complete understanding of REY environmental fate and anomalies cannot be achieved from the sole study of filterable water fractions (typically <0.45 μm).

1. Introduction

Lanthanides and yttrium (collectively referred to as REY) are powerful geochemical probes used to study igneous rock formation, continental crust evolution and chemical weathering, and to characterize the underlying lithologies of river waters at local and continental scales (e.g. McLennan, 1989, Elderfield et al., 1990; Sholkovitz, 1992; Dupré et al., 1996; Gaillardet et al., 2003; Bayon et al., 2015). REY mostly occur as trivalent cations except for Ce and Eu, which are redox sensitive. Specifically, Ce^{3+} can be oxidized to Ce^{4+} under oxic conditions, resulting in the formation of insoluble Ce oxides, whereas Eu^{3+} may be reduced to Eu^{2+} at elevated temperatures (above 200 °C) during the formation of hydrothermal fluids and/or melting (Brookins, 1989; Liu et al., 2017; Ingrao et al., 2019). For these reasons, the REY pattern of natural waters often bears Ce or Eu anomalies resulting from water-rock interactions or mineral dissolutions (Bau, 1999; Liu et al., 2017). In addition, Y and Ho are geochemical twins and have equal ionic radii (Brookins, 1989) and in the environment, a change in Y/Ho ratio can be due to REY scavenging to Fe or Mn (hydr)oxides (Bau, 1999; Ohta and Kawabe, 2001). Overall, REY are among the less mobile elements during weathering (Gaillardet et al., 2003) and are also highly particle-reactive (Merschel et al., 2017). A significant part of their so-called dissolved concentrations, which corresponds to an operationally-defined filterable fraction, is therefore often associated with colloids (Elderfield et al., 1990; Dupré et al., 1996; Gaillardet et al., 2003; Pokrovsky et al., 2006; Kulaksiz and Bau, 2013; Hissler et al., 2015a; Merschel et al., 2017).

Colloids can be defined as inorganic and organic (macro)molecules with at least one dimension between 1 nm and 1000 nm (Buffle and Leppard, 1995; Town and Filella, 2002). Although this operational, size-based definition neglects other important functional characteristics of colloidal matter, the key role of colloids in the biogeochemical cycles of trace elements is widely accepted (Gustafsson and Gschwend, 1997; Town and Filella, 2002; Vignati and Dominik, 2003; Gaillardet et al., 2003; Andersson et al., 2006; Stolpe et al., 2012). The role of colloids in determining the naturally fractionated REY patterns in filtered natural waters and in REY removal during estuarine mixing is well established (e.g. Elderfield et al., 1990; Sholkovitz, 1992; Kulaksiz and Bau, 2007; Davranche et al., 2015). However, relatively few studies have been published about REY fractionation and speciation along the particulate-colloidal-dissolved continuum, with most of them focusing on Boreal and Arctic rivers (Andersson et al., 2006; Stolpe et al., 2012). The possible role of colloids in REY speciation has also been directly documented in two large temperate rivers (Kulaksiz and Bau, 2013; Klaver et al., 2014), but only hypothesized in a peri-urban river heavily impacted by human activities (Hissler et al., 2014; Hissler et al., 2015a; Hissler et al., 2016). Furthermore, an accurate determination of the colloidal vs. truly dissolved REY levels strongly depends on the precision of the analytical determinations, because analytical errors during ICP-MS measurements will be propagated when calculating colloidal REY concentrations. The use of different techniques for separating colloids and true solutions (e.g., cross-flow filtration vs. centrifugal ultrafiltration) may also contribute to methodological errors that will affect the final accuracy of REY partitioning. To the best of our knowledge, no study has yet documented the effect of propagated analytical and methodological ultrafiltration errors on the quality of the REY fractionation patterns observed and on the REY anomalies calculated.

In recent years, REY have also emerged as technologically critical elements because of their widespread use in industrial activities, such as the production of supermagnets, catalysts, medicines, and in the automobile industry (Knobloch et al., 2018; Zhang et al., 2017), although the term critical actually derives from geopolitical rather than technological considerations (Zhang et al., 2017; Graedel et al., 2015). Anthropogenic uses of REY have been associated with REY anomalies in lakes, estuaries, rivers and groundwaters worldwide (e.g. Nozaki et al., 2000; Bau et al., 2006; Kulaksiz and Bau, 2007; Kulaksiz and Bau, 2013; Klaver et al., 2014; Merschel et al., 2015; Hissler et al., 2016). Since Bau and Dulski (1996), a positive Gd anomaly, related to the clinical use of Gd-based contrast agents in Magnetic Resonance Imaging (MRI), has been reported most frequently and is now considered worldwide as a distinctive signature of water inputs from wastewater treatment plants – WWTP (Bau and Dulski, 1996; Bau et al., 2006; Kulaksiz and Bau, 2011a; Merschel et al., 2015; Louis et al., 2020). Such an anomaly occurs because Gd-based contrast agents are not degraded during wastewater treatment due to their chemical stability (e.g. Verplanck et al., 2010; Parant et al., 2018). Gd-based contrast agents are also unreactive with environmental particles and the corresponding anomalies occur in the so-called "truly dissolved" fraction, defined by Kulaksiz and Bau (2013) as the fraction passing through 10 kDa ultrafiltration membranes. Other anthropogenic anomalies, notably La and Sm, have been reported in the colloidal fraction (operationally defined size range 10 kDa – 220 nm) or particulate fraction (Kulaksiz and Bau, 2013; Klaver et al., 2014). Hissler et al. (2016) identified a positive Nd anomaly in suspended particulate matter linked to steel manufacturing activities. Our future ability to univocally distinguish between natural vs. anthropogenically-driven REY fractionation and REY anomalies therefore depends, on the one hand, on an adequate knowledge of REY distribution among the truly dissolved, colloidal and particulate fractions and, on the other hand, on the fate of such anomalies according to hydrological condition changes. This is especially critical for urban and peri-urban river systems where inputs from WWTP often contribute significantly to the total water discharge. Moreover, the river basin connectivity, which controls the contribution of the different REY sources, can drastically change between low flows and flood conditions (Hissler et al., 2014; Hissler et al., 2015a; Barber et al., 2017).

In the present study, we examined the REY patterns in two human-impacted, small river basins having different lithology and land use, during low and high flow conditions. Specifically, (i) we analysed the REY concentrations in the particulate (>1000 nm), colloidal (1000 nm–200 nm and 200 nm–10 kDa) and dissolved (<10 kDa) fractions at both study sites and (ii) we quantified the associated analytical and methodological uncertainties on REY concentrations in each fraction. The results provide information on the links between hydrology and REY concentrations in river systems impacted by diverse anthropogenic activities and on the origin of the REY fractionation patterns in the different water fractions. These findings may be used to assess more precisely the impact of anthropogenic influences on REY geochemistry and the potential ecotoxicological effects of REY in contaminated rivers.

2. Material and methods

2.1. River water sampling

Samples were collected in the upstream part of the Alzette River basin, in the south-western part of Luxembourg. Two rivers were selected based on their contrasting geological setting and land cover (Pfister et al., 2017; SI-1). The cropland area, which is the most affected by soil erosion, and the agricultural practices can however be

considered as similar in both catchments (SI-1 Table S1). The upper Alzette River, highly impacted by urban and industrial activities, was sampled at Schifflange (AU) and in a wetland area located few kilometres downstream (WT). The sample collected at WT was only used to compare colloidal/dissolved separation techniques, as explained in Section 2.2.1. The Mess River basin, dominated by agricultural activities, was sampled at Pontpierre (MU). According to Wrede et al. (2015), the seasonality between precipitations and potential evapotranspiration in Luxembourg strongly affect the run-off regime. This generates low flows during summer (June to September) and high flows during winter (December to March). Consequently, the first sampling campaign was carried out on September 27, 2018 during low flow conditions and the second one on March 12, 2019 during high flow conditions. The river discharges were measured at each location during the sampling and were one order of magnitude higher during high flows compared to low flows (Table 1).The water electrical conductivity (TetraCond® 925, WTW), pH and temperature (SenTix® 940, WTW) were measured directly in the field (Table 1). All samples were stored at 4 °C before further treatments and analysis.

2.2. Sample preparation

2.2.1. REY partitioning among particulate, colloidal and dissolved fractions

We used a "cascade" filtration approach to isolate the following operationally defined fractions: the particulate fraction above 1000 nm, the coarse colloidal fraction between 1000 and 220 nm (CC in the rest of the document), the small colloidal fraction between 220 nm and 10 kDa (SC in the rest of the document) and the dissolved fraction, below 10 kDa. The threshold between the SC and the dissolved fractions roughly corresponds to a diameter of 2.8 nm for a spherical molecule (Erickson, 2009). Consequently, the dissolved fraction may contain some humic substance complexes that could be considered as colloids (Aiken et al., 2011; Lead and Wilkinson, 2006). All fraction separation steps were performed in clean laboratory conditions. All filtrations were performed in triplicates for solid residues (deposited on filters) while filtrates were pooled together by cut-off and stored in clean PP Nalgene® bottles. Membrane filters used to isolate the particulate and CC fractions were rinsed with 1 L of ultrapure water (Milli-Q, Millipore) immediately before their use. One liter of sample was first filtered at 1000 nm using a PTFE membrane (Omnipore™, Millipore, Ø47 mm) and then at 220 nm using a cellulose acetate membrane (Sartorius Stedim Biotech, Ø47 mm). The remaining 220 nm filtrate was separated into the SC and the dissolved fractions by centrifugal ultrafiltration (CU) using Amicon® Ultra-15 10 kDa (Millipore) units for 40 min at 4000 g (Heraeus Multifuge X3R, Thermo Scientific). The Amicon® units were cleaned beforehand with 0.5 M HCl followed by 0.1 M of NaOH. The units were rinsed twice with ultrapure water (Milli-Q, Millipore) after each cleaning step, which was sufficient to get the ultrafiltrate pH back to circumneutral values. Each centrifugal filter unit was preconditioned with 5 mL of sample (subsequently discarded) before the actual ultrafiltration of 15 mL sample aliquots was carried out. Ultrafiltration by CU was done in duplicate and (ultra)filtrates were pooled together beforehand to be acidified with HNO_3 to 1% and stored at 4 °C. Finally, the CU technique does not allow ultrafiltration mass balances to be established to check for possible contamination or losses during the separation process. The results obtained using CU were therefore compared with cross-flow ultrafiltration (CFF) using a Pellicon® XL Cassette Ultracel® 10 kDa (Millipore) for the WT sample only (SI-2).

2.2.2. Filter mineralization

The particulate and the CC fractions collected on the two types of filters, 1000 and 220 nm, respectively, were mineralized on a hot plate using an HNO_3-HF (12 h, T = 90 °C) / $HClO_4$ (12 h, T = 120 °C) / HNO_3 (12 h, T = 90 °C) acid mixture. This protocol allowed a total digestion of all type of inorganic and organic material in the sample collected on the filter membrane. The digested samples were then diluted with HNO_3 1% and stored at 4 °C before the ICP-MS analysis. In order to control the REY background that could originate from the filter

Table 1
River discharge (Q in L s^{-1}) and water physicochemical parameters measured at the Alzette (AU), Alzette wetland area (WT) and Mess (MU) study sites during low (LF) and high flows (HF) sampling campaigns. Dissolved Organic Carbon (DOC) measurements were performed in the <220 nm filtrate while the other physicochemical parameters in the <1000 nm filtrate fraction. The electric conductivity (EC) is in µS cm^{-1}, suspended particulate matter (SPM), DOC, cations and anions, particulate Fe and Al concentrations in mg L^{-1}, alkalinity in mol L^{-1} and colloidal and dissolved Al and Fe concentrations in µg L^{-1}. The errors on SPM and DOC concentrations are ±1 standard deviation (n = 3). N.D. = Not determined. <D.L. = Not detected.

	MU (HF)	MU (LF)	AU (HF)	AU (LF)	WT (LF)
Q	1630	20	1500	129	190
SPM	23.6 ± 7.2	54.0 ± 6.0	9.8 ± 2.8	12.3 ± 6.2	N.D.
DOC	5.4 ± 0.3	6.0 ± 0.1	N.D.	4.4 ± 0.2	7.4 ± 0.2
EC	458	820	760	895	975
pH	7.6	7.6	7.8	7.6	7.5
T (°C)	5.0	9.8	7.2	11.6	14.0
Alkalinity	2.45	4.97	3.26	3.78	3.57
Ca^{2+}	64.7	86.4	107.7	113.1	99.6
Mg^{2+}	4.7	8.2	7.7	9.4	9.0
K^{+}	3.4	11.7	12.3	12.8	21.1
Na^{+}	17.9	51.5	32.7	51.1	64.2
Cl^{-}	28.3	66.4	48.3	75.9	92.9
NO_3^{-}	3.5	0.4	1.1	1.9	5.6
PO_4^{3-}	0.2	2.5	0.2	0.8	2.3
SO_4^{2-}	40.0	57.6	137.7	132.8	129.5
Ionic balance (%)	4.1	4.5	1.7	1.0	0.3
Ionic strength (mol L^{-1})	0.006	0.010	0.011	0.012	0.012
Fe_P	1.5 ± 0.5	2.5 ± 0.4	0.6 ± 0.1	0.2 ± 0.1	2.9 ± 0.2
Al_P	2.5 ± 0.8	2.3 ± 0.9	0.6 ± 0.1	0.1 ± 0.1	3.1 ± 0.6
Mn_P	<D.L.	<D.L.	<D.L.	<D.L.	<D.L.
Fe_{CC}	104.3 ± 1.6	187.4 ± 12.8	6.9 ± 0.9	23.4 ± 4.7	N.D.
Al_{CC}	172.5 ± 3.8	27.9 ± 1.0	5.8 ± 0.8	1.8 ± 0.4	N.D.
Mn_{CC}	1.0 ± 0.1	4.2 ± 2.3	0.2 ± 0.1	0.4 ± 0.1	N.D.
Fe_{SC}	46.6 ± 0.9	114.9 ± 2.4	10.2 ± 0.2	69.5 ± 0.3	N.D.
Al_{SC}	34.2 ± 0.5	1.4 ± 0.5	1.2 ± 0.7	2.0 ± 0.8	N.D.
Mn_{SC}	<D.L.	<D.L.	<D.L.	4.9 ± 0.4	N.D.
Fe_D	4.5 ± 0.1	13.5 ± 0.2	5.6 ± 0.1	15.5 ± 0.1	15.0 ± 0.1
Al_D	5.4 ± 0.1	6.7 ± 0.4	18.5 ± 0.6	14.6 ± 0.2	6.6 ± 0.3
Mn_D	27.9 ± 0.1	472.6 ± 4.3	31.8 ± 0.1	67.9 ± 0.3	169.5 ± 0.5

composition, a series of blank filters were also prepared and mineralized following the same procedure (SI-3). HF (Suprapur 40%, Merck), purified HNO_3 (13.5 N - Savilex DST-1000) and $HClO_4$ (Suprapur 70%, Merck) were used for the mineralization and all dilutions were performed with ultrapure water (Milli-Q, Millipore).

The mass of a given element in the digested sample was calculated as follows (Eq. (1))

$$m_{meas} = ([X]_{meas} \times V_{digest}) - m_{blank} \quad (1)$$

with m_{meas} the mass of a given REY in μg; $[X]_{meas}$ the measured concentration by ICP-MS of the given REY in μg L^{-1}, V_{digest} the volume of the sample after dilution of the digested sample in L, and m_{blank} the mass of the given REY included in filter blanks in μg (SI-3).

2.3. Chemical analyses

The concentration of the suspended particulate matter (SPM) was determined gravimetrically after filtration at 1000 nm on the used PTFE Membrane filter that was subsequently dried in a desiccator until it reached a constant weight. The alkalinity (Mettler Toledo) and the major cations and anions (Dionex DX 500 and DX 600) were measured directly after filtration at 1000 nm. The dissolved organic carbon (Teledyn-Tekmar Apollo 9000) was measured after the filtration step at 220 nm. The river water composition is summarized in Table 1.

The REY, Al, Fe and Mn concentrations were analysed with a Quadrupole ICP-MS (Agilent 7900) associated with an ISIS 3 (Agilent) injection system. Analyses were conducted in He mode and ^{103}Rh and ^{185}Re were used as internal standards. Analytical blank values were less than 1% of the lowest sample concentrations for all elements. For all REY, the detection limit was 0.3 ng L^{-1} and the quantification limit was 1.0 ng L^{-1}. Calibration standards were prepared with Multi elements ICP standard solutions (CHEM-LAB Analytical) diluted in HNO_3 1%. One natural river water certified reference water (NRC-CNRC/SLRS-6) was analysed several times along the analytical series. Its REY concentrations are not certified but can be compared to Yeghicheyan et al. (2019). The values we obtained were between 91 and 101% of the published data (SI-4).

Some samples were expected to present low REY concentrations. They were pre-concentrated 5- to 8-fold before analysis by evaporation at 60 °C of the 1% HNO3 acidified initial liquid matrix. These samples were spiked with Tm to check for possible evaporative or adsorptive losses and Tm recoveries were between 98 and 104% (SI-5).

2.4. Calculation of the particulate and colloidal fractions

The average REY concentration in the particulate fraction (in μg L^{-1}) was estimated according to Eq. (2).

$$[X]_{Part} = \frac{1}{3}\sum_{i=1}^{3}\left(\frac{m_{meas,1000}}{V_{filt,1000}}\right)_i \quad (2)$$

with $[X]_{Part}$ the average of the concentration of a given REY in the three filter replicates in μg L^{-1}; $m_{meas,1000}$ the mass of the given REY deposited on one of the triplicate 1000 nm filters in μg (Eq. (1)), and $V_{filt,1000}$ the volume of water filtered for one filter triplicate in L.

Two different techniques were used to estimate the REY concentrations in the CC fraction. On the one hand, the REY bound to CC were estimated by subtraction between the concentrations measured in the filtrates at 1000 nm and 220 nm (Eq. (3)). On the other hand, the REY bound to CC were estimated directly using the concentration obtained from the 220 nm mineralized filters (Eq. (4)). Results comparing the subtraction and the mineralization techniques are gathered in SI-6. As the mineralization procedure delivered less uncertainty in the results, it will be used to present and discuss the REY content of the CC fraction.

$$[X]_{CC,sub} = [X]_{<1000} - [X]_{<220} \quad (3)$$

with $[X]_{CC,sub}$ the concentration of a given REY in the CC fraction obtained by subtraction between the REY content in the filtrates at 1000 nm and 220 nm in μg L^{-1}. $[X]_{<1000}$ is the measured concentration of the given REY in the filtrate below 1000 nm in μg L^{-1} and $[X]_{<220}$ is the measured concentration on triplicates of the given REY in the filtrate below 220 nm in μg L^{-1}.

$$[X]_{CC,min} = \frac{1}{3}\sum_{i=1}^{3}\left(\frac{m_{meas,220}}{V_{filt,220}}\right)_i \quad (4)$$

with $[X]_{CC,min}$ the average concentration on triplicates of a given REY in the CC fraction obtained after filter mineralization in μg L^{-1}, $m_{meas,220}$ the mass of the given REY deposited on a 220 nm filter in μg; $V_{filt,220}$ the volume of water filtered for one filter triplicate in L.

The SC fraction could only be estimated by subtraction between the REY concentrations measured in the filtrate at 220 nm and the ultrafiltrate at 10 kDa (Eq. (5))

$$[X]_{SC} = [X]_{<220} - [X]_{<10\ kDa} \quad (5)$$

with $[X]_{SC}$ the concentration of a given REY in the SC fraction in μg L^{-1}. $[X]_{<220}$ is the concentration of the given REY in the filtrate below 220 nm in μg L^{-1} and $[X]_{<10\ kDa}$ is the concentration of the given REY in the ultrafiltrate below 10 kDa in μg L^{-1}.

2.5. Calculation of the REY anomalies and the related anthropogenic contributions

All data presented in the following parts were normalized to Post-Archean Average Australian Shale (PAAS) from McLennan (1989). Cerium (Ce) and Neodymium (Nd) anomalies were calculated from Eqs. (6) and (7), respectively:

$$Ce_N/Ce_N^* = Ce_N/(0.5La_N + 0.5Pr_N) \quad (6)$$

$$Nd_N/Nd_N^* = Nd_N/(0.6Pr_N + 0.4Sm_N) \quad (7)$$

with Ce_N, Nd_N, La_N, Pr_N and Sm_N being the REY elemental concentrations normalized to PAAS.

Gadolinium (Gd) and Europium (Eu) anomalies were calculated based on the linear regression method described by Kulaksiz and Bau (2011b) and (Kulaksiz and Bau, 2013) who identified a linear trend between Pr_N, Nd_N and Sm_N. This trend is supposed to continue up to Gd_N in pristine rivers and thus allows the calculation of a Gd and Eu geogenic background, Gd_N^* (Eq. (8)) and Eu_N^* (Eq. (9); SI-7).

$$\log Gd_N^* = b_0 + b_1 x_{Gd} \quad (8)$$

Table 2
Estimation of the uncertainty (Δ) for the quantification of the REY parameters. Values obtained for each individual sample are presented in SI-8.

REY parameter	Uncertainty formula
$[X]_{meas}$, $[X]_{<1000}$, $[X]_{<220}$	Δ=Analytical error from ICP-MS measurement
$[X]_{Part}$, $[X]_{CC,min}$	$\Delta = SD = \sqrt{\frac{1}{(n-1)}\sum_{i=1}^{n}(x_i-\bar{x})^2}$ n = 3 (Eq. (11))
$[X]_{CC,sub}$, $[X]_{SC}$ using CU	$\Delta = \sigma_A = \sqrt{\sigma_B^2 + \sigma_C^2 + \ldots + \sigma_n^2}$ (Eq. (12))
$[X]_N$, REY anomalies, REY ratios, $[X^*]$, $[X_{ant}]$, $[X]_{SC}$ using CFF	$\Delta = \sigma_A^2 = A \times \sqrt{\left(\frac{\sigma_B}{B}\right)^2 + \left(\frac{\sigma_C}{C}\right)^2 + \ldots + \left(\frac{\sigma_n}{n}\right)^2}$ (Eq. (13))
$\log Gd_N^*$ and $\log Eu_N^*$	$\Delta = t_{(n-2)}\sigma_{xREY}$ n = 3 (Eq. (14))

SD = Standard Deviation.
$t_{(n-2)}$ and $\sigma_{x_{REY}}$ calculated as in Miller and Miller (2010).
Part: particulate fraction concentration in μg L^{-1}.
CC: coarse colloidal fraction concentration in μg L^{-1}.

$$\log Eu_N^* = b_0 + b_1 x_{Eu} \quad (9)$$

where x_{Gd} and x_{Eu} are the coefficients of the Pr_N, Nd_N and Sm_N linear regression obtained using the least squares method (Kulaksiz and Bau, 2011b). Anomalies are then quantified by the ratios Gd_N/Gd_N^* and Eu_N/Eu_N^*. The concentration of the anthropogenic contribution can be estimated from the geogenic background and the total concentration of the given REY (Eq. (10)).

$$[X_{ant}] = [X]_{total} - [X^*] \quad (10)$$

with $[X_{ant}]$ the anthropogenic concentration of a given REY that contributes to the total REY concentration in the sample; $[X]_{total}$ the total concentration of the given REY; $[X^*]$ the calculated geogenic concentration of the given REY.

2.6. Calculation of the errors

For each quantification, the corresponding uncertainties (Δ) were calculated from the standard deviation of replicate measurements (Eq. (11)) or using error propagation (Eqs. (12)-(14)) as summarized in Table 2. In the present study, we consider that analytical errors from ICP-MS measurements were the first level of uncertainty when calculating REY partitioning among the particulate, colloidal and dissolved fractions. The analytical errors are a function of each measured REY atomic mass and were obtained using Mass Hunter 4.4 software (Agilent technologies©) for 9 replicate measurements. Other sources of error arose from the weighing of volumes for V_{digest} (Eq. (1)), $V_{filt,1000}$ (Eq. (2)) and $V_{filt,220}$ (Eq. (4)), which presented an error of 0.0001, 0.01 and 0.01 g, respectively. Finally, for REY normalized to PAAS, no uncertainties are known for PAAS values. Thus, uncertainties for normalized concentrations only correspond to the propagation of uncertainties from measured REY concentrations (Eq. (13)).

To have more clarity about relative uncertainty, Δ was normalized by its parameter value to address the size of the uncertainty and was calculated as in Eq. (15):

$$E = \Delta / X \times 100 \quad (15)$$

with E the percentage of error varying between 0 and 100, Δ the uncertainty attached to X and X is the parameter of interest as summarized in Table 2 or as a volume (V_{digest}, $V_{filt,1000}$ and $V_{filt,220}$). Finally, the probability $p_{<10\%}$ of having an E value below 10% for a range of measured REY concentrations is calculated as in Eq. (16):

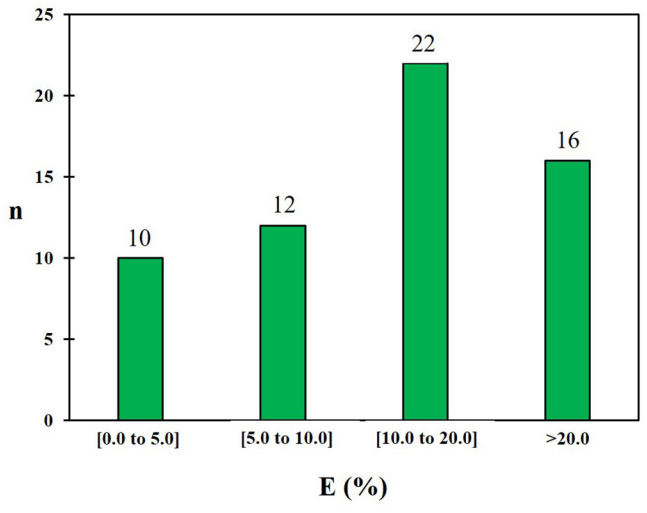

Fig. 1. Repartition of E (%) by classes (bars) in the small colloids and dissolved fractions. Total n value is 60 (see SI-8 for more details).

$$p_{<10\%} = n_{E_{<10\%}} / n_{E,tot} \quad (16)$$

with $p_{<10\%}$ the probability of having an E value below 10%; $n_{E,tot}$ the number of E values in the considered range of concentrations and $n_{E_{<10\%}}$, the number of E value below 10%. $p_{<10\%}$ has a value between 0 and 1.

3. Results

3.1. Analytical and methodological errors

3.1.1. Analytical errors

Measured concentrations are used for all calculations in this study. Dissolved and SC values are directly issued from them. Concentration values below 1 ng L^{-1} (except blanks) are always obtained after sample pre-concentration as described in Section 2.3 and SI-5. The 288 REY concentrations measured in this study range from 0.07 (blanks) to 10,498 ng L^{-1} (mineralized filters). E has a median value of 6%, an average of 10% and a standard deviation of 12%. However, E varies markedly depending on the measured concentrations. Between 10 and 20 ng L^{-1} $p_{<10\%}$ is 0.86 while it is 1.0 above 20 ng L^{-1}. Below 10 ng L^{-1} E is much more dispersed and ranges from 1.0 to 86%. The corresponding $p_{<10\%}$ value is 0.59 between 5 and 10 ng L^{-1} and falls to 0.17 below 1 ng L^{-1}. As could be expected, the lower the measured concentrations, the higher the probabilities of having high uncertainties (Fig. 1 and SI-8).

Sixty REY concentrations are measured and/or used to calculate SC and the dissolved fractions (Fig. 1). The concentrations are below 10 ng L^{-1} for 85% of the samples. Then, E is dispersed and presents 38 values above 10%. These E values explain the high uncertainties that might be observed on both SC and truly dissolved fractions (Fig. 1). This is particularly true for SC, which is calculated from two sample types and cumulates the uncertainties from the two concentrations used for its calculation (Eqs. (5) and (13)).

3.1.2. Error related to mineralization

Data resulting from the filter mineralization of the particulate and the CC fractions are calculated from three uncorrelated parameters (see SI-8): the filtrate volume, the digested volume and the measured concentration (Eqs. (1), (3) and (4)). Thus, the dispersion between triplicates, measured with SD in Eq. (12), depends on the variability of these three parameters. The measured REY concentrations in digested volumes are always above 10 ng L^{-1} and are mostly between 100 and 1000 ng L^{-1}. Such high concentrations correspond to lower uncertainties in comparison with the other water fractions. Consequently, the standard deviation estimated for the particulate and CC concentrations are principally due to the differences between the filtered volumes or the variations in the measured concentrations between replicates. Uncertainties are generally low in those two fractions (Fig. 2) because replicate samples can be very homogenous. However, higher uncertainties can be observed for AU during low flow. This would suggest higher heterogeneity for the analysed replicates (Fig. 2D).

3.2. Comparative performance of centrifugal (CU) and cross flow (CFF) ultrafiltration

The comparison was conducted only on WT and MU samples collected during the low flow sampling campaign (Table 1). The REY patterns for the CFF permeate and the CU ultrafiltrate are very similar for the colloidal and dissolved fractions. For the latter, the CFF concentrations from La to Tm are always smaller, with the difference progressively decreasing along the lanthanide series and disappearing for Yb and Lu. Consequently, La_N/Yb_N ratios differ for CU (0.03 ± 0.01 and 0.02 ± 0.01 for WT and MU, respectively) and CFF (0.004 ± 0.001 and 0.012 ± 0.002 for WT and MU). The Gd_N values are also equal for the two techniques (Fig. 3A and 3C). The CFF mass balances range from 42 to 47% for light REY (LREY: La to Nd), from 38 to 53% for medium REY (MREY: Sm to Dy), except for Gd (85 to 103%) and from 46 to 92% for

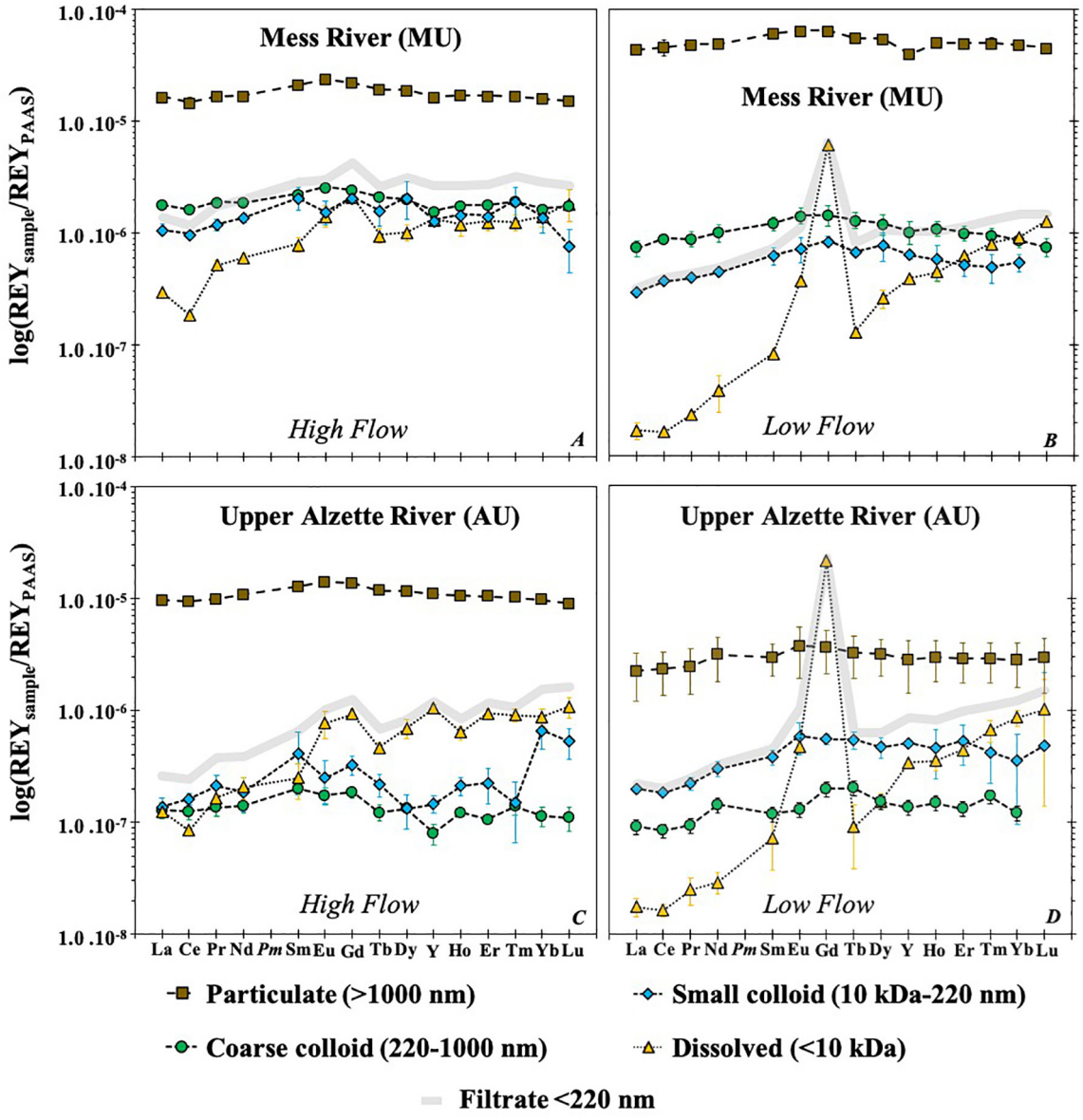

Fig. 2. PAAS-normalized REY patterns for particulate, coarse and small colloidal and truly dissolved fractions in the Mess River (MU) during high flow (A) and low flow (B) and in the upper Alzette River (AU) during high flow (C) and low flow (D). The error bars correspond to 2Δ. Raw concentration data used to calculate PAAS-normalized REY patterns are gathered in SI-9.

heavy REY (HREY: Ho to Lu; Fig. 3A and 3C). Errors, expressed as 2Δ, are higher for CFF than for CU in particular for Pr, Nd, Sm, Tb, Ho and Lu (Fig. 3A and 3C).

In Figs. 3B and 3D, the colloidal fraction corresponds to all colloids between 10 kDa and 1000 nm. For CU, those values are obtained by subtracting the concentration below 10 kDa from the concentration below 1000 nm, whereas with CFF separation technique, the colloidal concentrations are directly measured in the retentate (see SI-2). However, the REY colloidal concentrations remain 2 to 5 times higher for CU than for CFF. Finally, errors linked to the colloidal fractions are similar and small for all patterns except for Gd and Lu in CFF at the WT sampling site (Fig. 3B). Unless otherwise specified, only results from CU will be further used to discuss the distribution of REY in the present work.

3.3. REY concentrations in the Mess River: marls dominated by agricultural landscape

With the exception of Gd and some HREY, the REY are more concentrated in the particulate fraction and progressively decrease from CC to the dissolved fraction in both hydrological conditions (Fig. 2).

During high flows, the particulate fraction presents lower REY concentrations than in low flow conditions with a similar PAAS-normalized pattern. The particulate and CC fractions also exhibit very similar patterns. SC is slightly more depleted in LREY than CC and presents a small Eu anomaly (Table 3) and a Lu depletion (Fig. 2A). The dissolved pattern is strongly depleted in LREY compared to the other fractions, as shown by $La_N/Yb_N = 0.21 \pm 0.01$ and $La_N/Eu_N = 0.20 \pm 0.05$ (Table 3). Positive Eu and Gd anomalies are observed in the dissolved fraction with values of 1.56 ± 0.40 and 2.00 ± 0.26, respectively (Fig. 2A and Table 3). Gd_{ant} represents $50 \pm 10\%$ of the total Gd concentration in this fraction (Table 3). A negative Ce anomaly of 0.46 ± 0.04 can be observed in the dissolved fraction (Fig. 2A and Table 3). Finally, Gd positive and Ce negative anomalies in the <220 nm filtrate fraction are less pronounced (Fig. 2A) and closer to 1 (Table 3) compared to the dissolved.

During low flows, the particulate and CC fractions present a similar pattern with a small enrichment in MREY (Fig. 2B and Table 3). $La_N/Yb_N = 0.85 \pm 0.26$ and $Eu_N/Yb_N = 1.65 \pm 0.50$ in CC are similar to the ratios in particulate, but $La_N/Eu_N = 0.51 \pm 0.17$ differs and indicates a more fractionated pattern in CC than in particulate (Table 3). The SC

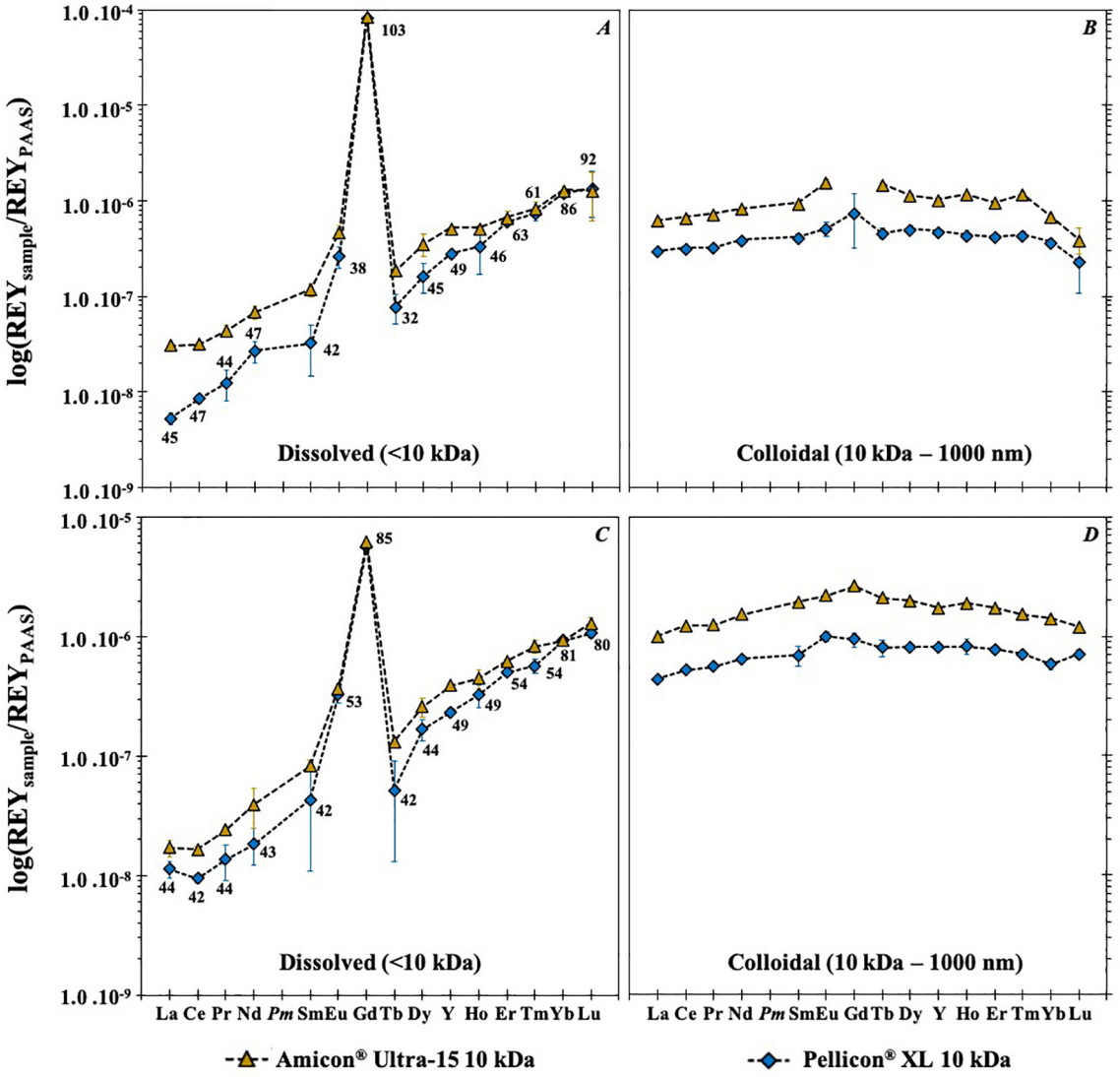

Fig. 3. Comparison of PAAS-normalized REY patterns in low flow conditions. (A) and (B) present the dissolved fraction (< 10 kDa) and the colloidal fraction (10 kDa to 1000 nm), respectively, for the Alzette River at WT (cf = 8.9). (C) and (D) present the dissolved and the colloidal fractions, respectively, for the Mess River at MU (cf = 7.0). The numbers indicated in (A) and (C) correspond to the recovery yield obtained with the CFF technique (see also SI-2). Indicated error bars are 2Δ.

pattern is more depleted in LREY than particulate and CC fractions with $La_N/Yb_N = 0.55 \pm 0.11$ and $Eu_N/Yb_N = 0.41 \pm 0.11$. The pattern of the dissolved fraction is strongly depleted in LREY in comparison to HREY as outlined by $La_N/Yb_N = 0.02 \pm 0.01$ and $Eu_N/Yb_N = 0.40 \pm 0.05$. Positive Eu and Gd anomalies can be observed in the dissolved fraction with values of 2.90 ± 0.56 and 32.2 ± 4.4, respectively (Fig. 2B and Table 3). Gd_{ant} represents 97 ± 2% of the total Gd (Table 3). The patterns of the <220 nm filterable fractions are less fractionated as they integrate the combined characteristics of dissolved and SC fractions (Fig. 2A and 2B; Table 3). As an example, the positive anomalies in Gd and Eu are also identified but with lower intensity than for the dissolved fraction (Fig. 2B and Table 3).

3.4. REY concentrations in the upper Alzette River: limestones and marls dominated by urban and industrial landscapes

During high flow, the particulate fraction presents higher REY concentrations than in low flow conditions with a similar PAAS-normalized pattern. Furthermore, LREY concentrations are very close between the dissolved, CC and SC fractions with higher MREY and HREY concentrations observed in the dissolved fraction (Fig. 2C). The SC fraction is more concentrated than its corresponding CC fraction and the SC pattern is more fractionated and presents more uncertainties and fluctuations than the CC (Fig. 3C and Table 3). In the SC fraction, Yb and Lu are enriched compared to other REY ($La_N/Yb_N = 0.21 \pm 0.11$) and REY normalized concentrations increase from La to Sm and then decrease from Eu to Dy (Fig. 2C). A negative Eu anomaly is present in both colloidal fractions (SC: 0.22 ± 0.09 and CC: 0.74 ± 0.14). Finally, the dissolved pattern remains depleted in LREY as shown by the $La_N/Yb_N = 0.14 \pm 0.03$ and $La_N/Eu_N = 0.16 \pm 0.05$ ratios (Table 3). Positive Eu and Gd anomalies are observed in the dissolved fraction with values of 2.61 ± 0.81 and 2.77 ± 0.42, respectively. Gd_{ant} represents 64 ± 12% of the total Gd concentration in the dissolved fraction (Table 3). A negative Ce anomaly ($Ce_N/Ce_N^* = 0.58 \pm 0.07$) is noticed for the dissolved fraction (Fig. 2C and Table 3). The pattern of the <220 nm filtrate fraction is similar to that of the dissolved, although it is less fractionated between LREY and HREY and with lower REY anomalies (Fig. 2C and 2D; Table 3).

During low flow, a positive Nd anomaly is detected in both particulate and CC (Fig. 2D and Table 3) due to a Nd concentration increase, as shown by the Sm_N/Nd_N ratio below 1. The CC and SC patterns present a small MREY enrichment and a slight depletion in LREY with $La_N/Yb_N =$

Table 3
PAAS-normalized REY ratios, anomalies and related anthropogenic concentrations for the different fractions at each sampling location. The errors are in italic and correspond to 1Δ. Raw concentration data used to calculate ratios are gathered in SI-9.

	Size	MU (HF)	MU (LF)	AU (HF)	AU (LF)
La_N/Yb_N	Particulate	1.03 ± *0.17*	0.91 ± *0.19*	0.99 ± *0.05*	0.79 ± *0.70*
	CC	1.09 ± *0.10*	0.85 ± *0.26*	1.12 ± *0.42*	0.76 ± *0.23*
	SC	0.77 ± *0.25*	0.55 ± *0.11*	0.21 ± *0.11*	0.57 ± *0.43*
	Dissolved	0.21 ± *0.01*	0.02 ± *0.01*	0.14 ± *0.03*	0.02 ± *0.01*
	<220 nm filtrate	0.49 ± *0.09*	0.21 ± *0.01*	0.17 ± *0.05*	0.18 ± *0.02*
La_N/Eu_N	Particulate	0.69 ± *0.18*	0.67 ± *0.12*	0.69 ± *0.06*	0.60 ± *0.56*
	CC	0.70 ± *0.04*	0.51 ± *0.17*	0.73 ± *0.32*	0.71 ± *0.21*
	SC	0.69 ± *0.24*	0.41 ± *0.11*	0.55 ± *0.35*	0.34 ± *0.12*
	Dissolved	0.20 ± *0.05*	0.05 ± *0.01*	0.16 ± *0.05*	0.04 ± *0.01*
	<220 nm filtrate	0.46 ± *0.05*	0.25 ± *0.04*	0.26 ± *0.08*	0.21 ± *0.03*
Eu_N/Yb_N	Particulate	1.48 ± *0.22*	1.35 ± *0.26*	1.45 ± *0.19*	1.33 ± *1.22*
	CC	1.56 ± *0.15*	1.65 ± *0.50*	1.53 ± *0.46*	0.87 ± *0.26*
	SC	1.11 ± *0.58*	1.33 ± *0.58*	1.20 ± *0.90*	1.66 ± *1.74*
	Dissolved	1.01 ± *0.43*	0.40 ± *0.05*	4.58 ± *2.07*	0.55 ± *0.13*
	<220 nm filtrate	1.06 ± *0.10*	0.74 ± *0.14*	0.66 ± *0.20*	0.87 ± *0.21*
Ce_N/Ce_N^*	Particulate	0.88 ± *0.19*	1.00 ± *0.29*	0.96 ± *0.06*	1.00 ± *0.87*
	CC	0.88 ± *0.02*	1.10 ± *0.29*	0.94 ± *0.30*	0.91 ± *0.27*
	SC	0.86 ± *0.15*	1.06 ± *0.06*	0.93 ± *0.32*	0.87 ± *0.12*
	Dissolved	0.46 ± *0.04*	0.81 ± *0.13*	0.58 ± *0.07*	0.78 ± *0.28*
	<220 nm filtrate	0.76 ± *0.07*	1.05 ± *0.05*	0.77 ± *0.17*	0.86 ± *0.08*
Eu_N/Eu_N^*	CC	–	–	0.74 ± *0.14*	0.80 ± *0.15*
	SC	0.63 ± *0.18*	0.99 ± *0.29*	0.22 ± *0.09*	1.22 ± *0.44*
	Dissolved	1.56 ± *0.40*	2.90 ± *0.56*	2.61 ± *0.81*	4.55 ± *0.75*
	<220 nm filtrate	0.89 ± *0.06*	1.31 ± *0.23*	1.27 ± *0.26*	1.85 ± *0.35*
Sm_N/Nd_N	Particulate	1.25 ± *0.18*	1.23 ± *0.23*	1.18 ± *0.07*	0.94 ± *0.70*
	CC	1.20 ± *0.04*	1.21 ± *0.38*	1.43 ± *0.29*	0.83 ± *0.25*
Nd_N/Nd_N^*	Particulate	0.92 ± *0.14*	0.92 ± *0.18*	0.98 ± *0.06*	1.18 ± *0.57*
	CC	0.92 ± *0.03*	0.99 ± *0.32*	0.87 ± *0.22*	1.39 ± *0.42*
Gd_N/Gd_N^*	Dissolved.	2.00 ± *0.26*	32.2 ± *4.4*	2.77 ± *0.42*	141 ± *16*
	<220 nm filtrate	1.05 ± *0.11*	6.20 ± *0.48*	1.27 ± *0.20*	32.07 ± *2.19*
Nd_{ant} (ng L^{-1})	Particulate	0.0	0.0	0.0	16.4 ± *80.0*
	CC	0.0	0.0	0.0	1.36 ± *1.26*
Nd^* (ng L^{-1})	Particulate	574 ± *48*	1684 ± *161*	368 ± *11.0*	89.4 ± *34.5*
	CC	63.4 ± *1.3*	34.3 ± *6.0*	4.76 ± *0.65*	3.51 ± *0.53*
Eu_{ant} (ng L^{-1})	Dissolved	0.55 ± *0.38*	0.36 ± *0.05*	0.51 ± *0.24*	0.40 ± *0.05*
Eu^* (ng L^{-1})	Dissolved	0.99 ± *0.04*	0.14 ± *0.01*	0.32 ± *0.01*	0.11 ± *0.01*
Gd_{ant} (ng L^{-1})	Dissolved	4.95 ± *1.07*	28.1 ± *0.7*	2.78 ± *0.54*	99.4 ± *0.5*
Gd^* (ng L^{-1})	Dissolved	4.93 ± *0.23*	0.90 ± *0.11*	1.57 ± *0.06*	0.71 ± *0.08*

0.76 ± 0.23 and La_N/Yb_N = 0.57 ± 0.43, respectively. CC also presents a small negative Eu anomaly (0.85 ± 0.15) (Fig. 2D and Table 3). The dissolved pattern is strongly depleted in LREY, as marked by La_N/Yb_N = 0.02 ± 0.01 and Eu_N/Yb_N = 0.55 ± 0.13 (Table 3). Positive Eu and Gd anomalies are observed in the dissolved fraction with values at 4.6 ± 0.8 and 141 ± 16, respectively (Fig. 2D and Table 3). Gd_{ant} represents 99 ± 0.5% of the total Gd in this fraction (Table 3and Fig. 2D). The pattern of the <220 nm filtrate fraction is similar to that of the dissolved fraction, although less fractionated between LREY and HREY and with lower REY anomalies (Fig. 2C and 2D; Table 3).

4. Discussion

4.1. Comparative performance of the two REY separation techniques for the small colloids and the dissolved fractions

The differences in the REY patterns of the colloidal and dissolved fractions indicate that the simple separation between particulate and filterable fractions cannot capture the full complexity of REY behaviour in the studied river waters. Therefore, the separation between colloidal and dissolved REY is an important step before characterizing and quantifying anthropogenic REY anomalies.

The CU and CFF device used in the present study have the same membrane type (regenerated cellulose) and the same nominal cut-off of 10 kDa according to the manufacturer specifications (Millipore). A good agreement between nominal and actual membrane cut-off was confirmed experimentally by Larsson et al. (2002) for the Pellicon XL CFF devices used in the present study, while no analogous information exists for CU. Previous research suggests that no systematic differences in the elemental partitioning between colloids and the true solution are obtained using regenerated cellulose membranes with different surface areas (Kottelat et al., 2008). The different dissolved REY concentrations obtained by CFF and CU in the present study may indicate an overestimation of dissolved REY by CU following membrane saturation or breakthrough of small colloids. Alternatively, losses of small colloids (<10 kDa) or the adsorption of dissolved molecules onto the CFF membrane may lead to an underestimation of dissolved REY when using this technique. The colloidal losses in CFF can originate from i) hydrodynamic effects (i.e., concentration polarization at the membrane surface) or/and ii) chemical interactions between macromolecules and the membrane surface (Larsson et al., 2002).

Artefacts linked to hydrodynamic effects can be practically eliminated by using a cross-flow ratio higher than 15, while membrane-macromolecule interactions may be minimized by using a CFF concentration factor above 10. The cross-flow ratio is defined as the ratio between the sample flux in the retentate line divided by the sample flux in the permeate line. The concentration factor is the ratio between the initial sample volume of filtered water to be fractionated by CFF and the retentate volume at the end of the fractionation (SI-2 Eq. A2). Our experimental procedure satisfied the first condition with cross-flow ratios that were always larger than 20 but fell slightly short of the second condition with concentration factors between 7.0 and 8.9. Note that high concentration factors also reduce errors when calculating the

colloidal fraction at the end of the CFF (SI-2 Eq. A2). However, differences between permeate and retentate were always high in our experiments and errors on the calculated colloid concentrations remained low (SI-2 for data). On the other hand, the particles with a size close to that of membrane pores could have been partially retained by the CFF membrane because of a concentration factor of less than 10.

The likelihood of a possible membrane saturation during ultrafiltration using CU was verified by comparing two different ultrafiltration procedures for the Amicon® Ultra 15 10 kDa device. In the present study, 30 mL of the dissolved fraction were necessary to perform the various analytical determinations. In a first procedure, this volume was obtained by 2 successive 15 mL ultrafiltration with the same membrane, while 2 different membranes were used for the second procedure. No differences were observed between the two procedures (SI-10 Fig. S5), implying that the first procedure did not saturate the Amicon® membranes and that the differences observed between CU and CFF should not be caused by methodological artefacts when using the CU procedure.

CFF mass balances for major cations, anions, manganese and gadolinium were constantly above 90% (SI-2 CFF excel file). These elements usually occur as dissolved (ionic) species or small inorganic complexes, suggesting that adsorption losses to the CFF membrane can be considered negligible. Organic carbon also showed a good mass balance (SI-2 CFF excel file), confirming that small organic complexes were not trapped by the CFF membrane either. Conversely, elements known to form (hydro)oxides in the colloidal-size range, such as Fe or Al (Town and Filella, 2002; Gaillardet et al., 2003), have recoveries between 45 and 65% only (SI-2 CFF excel file), close to those of most of the REY (Fig. 3A and 3B). Thus, the observed REY poor mass balances for CFF likely arise from "losses" of the colloidal fraction during the separation procedure. This hypothesis is also geochemically coherent with the REY fractionation observed in the dissolved fraction (Fig. 3A and 3C). For HREY, CFF recoveries are up to 92% (SI-2 in the Excel file) and the dissolved concentrations are similar between CU and CFF, in agreement with the higher affinity of HREY for organic colloids (Tang and Johannesson, 2003; Pourret et al., 2007a; Pourret et al., 2007b; Pourret et al., 2007c). On the contrary, the low CFF recoveries and the marked differences between the two techniques indicate the more important role that Fe and Al colloids (i.e. clay nanoparticles, ox(hydro)ides, Fe/humic complexes) could play as MREY and LREY carries. These macromolecules could react with the CFF membrane as previously discussed.

Despite these differences, both techniques yield a similar fractionation pattern along the lanthanide series and point to the common occurrence of a significant colloidal REY fraction in the <220 nm filtrate. It remains however a matter of speculation as to whether the most accurate dissolved REY concentrations are provided by CU or CFF. If the 'losses of colloidal REY' are the sole cause of poor CFF mass balances, the dissolved concentrations obtained by CFF may be as valid as those obtained by CU. However, no definite decision can be made a priori as to the colloidal of dissolved nature of CFF 'losses' (Steinmann et al., 1999). For this reason, we chose to base the discussion in this paper on dissolved results obtained by CU. Johnsen et al. (2016) showed that the Amicon® Ultra 15 10 kDa can retain proteins larger than their nominal cut-off, but their experimental procedure did not allow them to confirm the actual membrane cut-off. The permeability of CU units to colloids having a size close to the nominal cut-off cannot therefore be excluded.

The CU technique presents a practical interest due to its ease of use in comparison to CFF, especially during flood events when high frequency sampling (from minutes to hours) is necessary to accurately study the REY partitioning between colloidal and dissolved fractions. A community-level effort is clearly needed to correctly calibrate CU devices before accumulating a large set of data without adequate quality control procedures on the accuracy of REY fractionation procedures.

4.2. New insights for the anthropogenic impact on REY in rivers

Except for SC, all fractions contain a REY anomaly that could be ascribed to an enrichment originating from a specific anthropogenic use of a given lanthanide. The most enriched anthropogenic REY (AREY) is Gd, which is used as a contrast agent in MRI exams (Bau and Dulski, 1996). The dispersion process of Gd_{ant} from the WWTP to the aquatic systems is now quite well documented (Bau and Dulski, 1996; Möller and Dulski, 2010; Kulaksiz and Bau, 2011b; Merschel et al., 2015). Anthropogenic inputs of Gd in the upper Alzette River basin have been previously reported (Hissler et al., 2014; Hissler et al., 2016; Hostache et al., 2014). During low flow conditions, our results are similar to those of Kulaksiz and Bau (2013), who concluded that Gd_{ant} in the Rhine River is only present in the dissolved fraction (<10 kDa) and does not react with environmental particles either in the WWTP or in the river system downstream of the WWTP effluent. The present study shows that the Gd_{ant} concentration in the dissolved fraction (<10 kDa) varies markedly in the two contrasting hydrological conditions studied. The Gd anomaly is much higher during low flow than high flow (Table 3 and Fig. 2). In low flow, the Gd_{ant} concentration represents 99% and 97% of total Gd in the dissolved fraction at AU and MU sampling sites, respectively (Fig. 2B and 2D). However, during high flow conditions, the Gd_{ant} content in the dissolved fraction decreases to 64% and 50% of the total Gd concentration in the solution, respectively (Fig. 2A and 2C). The river hydrology clearly plays a crucial role regarding the dilution of dissolved Gd_{ant}. When the river discharge increased, the concentration of dissolved LREY and MREY increased in comparison to the HREY (Fig. 2). This different behaviour between REY was illustrated by the significant increases of the La_N/Yb_N and Eu_N/Yb_N ratios during high flow at both sites (Table 3). This LREY and MREY contribution can be caused by more natural sources (e.g. eroded soil particles and colloids) that are mobilized in different parts of the catchment and transported in the river bed when the hydrological connectivity is activated during flood events and by mobilization of riverbed sediments. As for the other LREY and MREY, a natural Gd contribution entered the composition of the dissolved fraction during high flow. Natural dissolved Gd concentration increased by factors of 5.5 and 2.2 for MU and AU respectively (Table 3). This new Gd input may occur as ionic species or in association with humic substances smaller than 10 kDa that remain operationally included in the dissolved fraction. This result also highlighted that the REY partitioning in the filterable fraction (<220 nm) integrates the different characteristics of both colloids and dissolved components, partly masking the true extent of REY anthropogenic anomalies.

The dissolved fraction also shows a significant positive Eu anomaly in both hydrological conditions although it is more important during low flows like for Gd (Table 3 and Fig. 2). To the best of our knowledge, it is the first time that such a positive anomaly is described for Eu in the dissolved fraction of contaminated rivers. Other data published on anthropogenically impacted river basins could have an Eu positive anomaly in their filtered fractions (e.g. Nozaki et al., 2000; Klaver et al., 2014; Tepe et al., 2014) without any mention made of it. Besides this, considering only the <220 nm (or higher) filtrate fraction could considerably limit the observation of a positive Eu anomaly as it is mostly visible in the dissolved one (<10 kDa), as highlighted by Fig. 2 and Table 3. The first explanation of the Eu anomaly could be spectral interferences of ^{153}Eu with ^{137}Ba and ^{136}Ba oxides (Smirnova et al., 2006). However, during our analysis, SRLS-6 average recoveries for ^{153}Eu were 95 ± 2% ($n = 5$; SI-4), excluding possible analytical interferences. A second explanation could be related to a redox change from Eu^{3+} to Eu^{2+}. Such changes usually take place during melting processes at high temperatures (e.g. Liu et al., 2017; Ingrao et al., 2019), but bacterial reduction of Eu^{3+} has also been observed (Maleke et al., 2019). A third explanation could be the transmetallation from Gd_{ant} chelates in the WWTP process, which could occur in our systems due to the major differences between Gd_{ant} and Eu concentrations (Möller and Dulski, 2010). Moreover, an Eu positive anomaly is present only in the dissolved fraction as

it is the case for Gd_{ant} (Fig. 2). The available results do not allow us to choose definitively between the three explanations until a more detailed study has been performed to elucidate the potential anthropogenic sources of Eu in polluted river systems.

The particulate and CC fractions of the upper Alzette River carry anthropogenic Nd (Nd_{ant}) (Table 3 and Fig. 2D). During this study and contrary to the observations of Hissler et al. (2016), the corresponding anomalies were only visible during low flows (Table 3, Fig. 2D) and were characterized by a high level of uncertainty (Table 3). In addition, the Nd/Nd^* and the Sm_N/Nd_N ratios indicate a higher Nd concentration in comparison to all other samples (Table 3). Hissler et al. (2016) attributed this enrichment to Nd inputs coming from past and/or current steel making activities. This assumption was based on a specific $^{143}Nd/^{144}Nd$ isotopic ratio that was closer to the isotopic compositions of steel plant emissions than to all other suspended sediment sources of the upper Alzette River basin. The presence of a specific anthropogenic source of Nd connected to the river is the only possibility of reaching such a distinct $^{143}Nd/^{144}Nd$ signature in the river itself and explaining the high uncertainty associated with the Nd anomaly compared with the other AREY. We surmise that only a specific source of Nd, instead of a diffuse one, can generate such a high heterogeneity in the sample replicates. Nevertheless, for the moment, these results are not able to rigorously identify the nature of the specific phase that controls the presence of Nd_{ant} in the particulate and CC fractions of the Alzette River. Although the use of big magnets, heavily enriched in Nd, during steel production represents a likely source of Nd_{ant}, the mechanisms responsible for such a high fractionation for Nd require further investigations of the processes used in steel factories.

4.3. Changes in REY patterns in polluted rivers in contrasted hydrological conditions and land uses

In the rivers studied, each of the PAAS-normalized REY patterns of particulate, colloidal and dissolved water fractions presented very specific characteristics. Overall, LREY gradually became depleted from the particulate to the dissolved fraction as confirmed by the corresponding decrease in La_N/Yb_N and La_N/Eu_N ratios (Table 3). The extent of LREY depletion in each fraction is also related to the river flow. This observation can be generalized for the two river catchments studied, which present contrasted land use but a certain similarity regarding the geological composition and the soil properties of agricultural lands. The PAAS-normalized REY patterns of the different fractions look like a continuum between two end-members: the particulate and dissolved fractions, whose contributions depend on the hydrological conditions.

For both rivers, most of the REY are in the particulate fraction, independent of hydrological conditions (Fig. 2). For instance, the particulate La represents between 84% (MU high flow) and 98% of the total La (MU low flow) while the particulate Yb contributes between 68% (AU low flow) and 95% of total Yb (MU low flow). However, one exception is observed for AU during low flow where 82% of total Gd is in the dissolved fraction (Fig. 2D). The particulate shows the same pattern with a slight MREY enrichment, in agreement with the similar lithologies (Lias marls and limestones) and soils in both catchments and regardless of the hydrological conditions (Fig. 2). It means that during our samplings, the particulate REY fractions have similar sources, except for the small anthropogenic contribution of Nd at AU. The primary origin of those REY comes from the erosion of soil particles by run-off occurring mainly in cropland during long and intense rain fall events, when the lands are hydrologically connected to the river. An additional source could also be the mobilization of riverbed sediment but most of these particles stored on the riverbed after flood events might have a similar origin and present same REY characteristics. As proposed by Hissler et al. (2016), a non-negligible phosphate component (as natural primary or secondary minerals or fertilizer input), could be considered to explain the MREY enrichment. However, the patterns observed are also close to the PAAS-normalized ones of clay suspended sediments (≤2 μm) in river systems draining sedimentary bedrocks (Bayon et al., 2015), which is also concordant with the lithological and soil composition of the Alzette River basin. Such a pattern suggests a close link between transported particulate REY and the presence of clay minerals in the river channels, because clays generate very similar patterns (Coppin et al., 2002; Yang et al., 2019). Additionally, it appears that hydrological conditions can modify particulate REY concentrations (mass of REY in the water column in $\mu g\ L^{-1}$) and loads (mass of REY in the suspended particulate matter in $\mu g\ g^{-1}$) which both change according to the hydrological conditions, but in different ways (Table 1 and Fig. 2). In the upper Alzette River, the REY load changes from $46 \pm 4\ \mu g\ g^{-1}$ to $253 \pm 77\ \mu g\ g^{-1}$ in low and high flows, respectively. It appears that particles with higher content in REY are in suspension during high flow, which explains the higher concentrations observed in Fig. 2C and 2D. During our sampling in the Mess River, particulate REY concentration is higher in low flows than in high flows (Fig. 2A and 2B). This high concentration of particulate REY (in $\mu g\ L^{-1}$) during low flow for a significantly lower river discharge (Table 1) is unusual in comparison to high flow. It can be explained by work on the bank of the river, in a region where soil sealing due to urbanization is still increasing. This can release more particles than usual in the water during low flow sampling. However, the loads of REY remain similar during both hydrological conditions with $\sum$REY ranging from $185 \pm 22\ \mu g\ g^{-1}$ to $152 \pm 33\ \mu g\ g^{-1}$, respectively. Despite the unexpected high suspended sediment concentration during low flow in the Mess River, same nature of particles seems to be transported regardless of the hydrological conditions. This indicates the role of land use on the transport of particulate REY. While both basins share similar geology, the upper Alzette River basin presents land use composed of 27, 54, and 19% of forest, agricultural land and urban/industrial areas, respectively, whereas the Mess River drains a basin composed of 9, 81 and 10% of forest, agricultural land and urban areas without any industry, respectively (SI-1). These main differences in agriculture and industry contributions to the land cover of the two catchments may explain the difference in the particulate REY loads and composition between high and low flow periods.

The largest fractionation between LREY and HREY is observed for the dissolved fraction, especially during low flows (Fig. 2) as already mentioned by Kulaksiz and Bau (2013) and the references therein. More precisely, the La_N/Yb_N and La_N/Eu_N ratios are below 0.1 in low flow (Table 3), while they slightly increase during high flow (Table 3). Moreover, MREY are also depleted compared to HREY during low flows, as illustrated by low Eu_N/Yb_N ratios (Table 3) whereas this depletion is lost during high flows (Table 3). This can only be attributed to a change in the source of dissolved LREY between the two hydrological conditions. In low flow conditions, the dissolved REY patterns appear to bear a typical WWTP-fingerprint (SI-11). These results prove that during the driest periods of the year, the WWTP effluents are the main source of dissolved REY in these two peri-urban rivers. On the contrary, when high flows occur, with the complete hydrological connection throughout the basins, more natural sources become the main contributors to the REY budget in the two rivers. During this period, the WWTP fingerprint is diluted by the natural fingerprints and the LREY vs. HREY fractionation is significantly reduced (Table 3). This is strengthened by the negative Ce anomaly, observed during high flows (Fig. 2), which is usually related to basin geology, soil solution and/or groundwater contributions (Dia et al., 2000; Gruau et al., 2004; Pédrot et al., 2008; Pourret et al., 2010; Hissler et al., 2015b; Pédrot et al., 2015; Louis et al., 2020).

The CC patterns remain poorly fractionated and more similar to those of the particulate fraction, albeit more than 1000-fold less concentrated (Table 3 and Fig. 2). During both high and low flow periods, La_N/Yb_N, La_N/Eu_N and Eu_N/Yb_N ratios are equal between CC and the particulate fractions. This suggests that the nature of REY-bearing particles is similar for CC and the particulate fractions and that only their sizes differ (Table 3, Fig. 2). On the contrary, SC patterns are more depleted in LREY than CC and, consequently, the particulate fraction (Fig. 2). This depletion in LREY can be attributed to a change in the nature of colloids

between CC and SC fractions. Indeed, when the colloidal size decreases, colloids tend to change from bio-organo-mineral micro-aggregates, as the CC fraction could be in this study, to amorphous oxides and organic complexes (of variable size and nature) such as humic or fulvic acids and proteins (Lead and Wilkinson, 2006), as the SC fraction could be. REY adsorption onto minerals or their complexation to ligands are quite complex processes and have a direct impact on the REY fractionation observed (Bau, 1999; Ohta and Kawabe, 2001; Davranche et al., 2004; Davranche et al., 2005; Davranche et al., 2008). In the Mess River, the data acquired during low flows should be carefully used as it is difficult to predict the impact of the unexpected high suspended sediment concentration on the CC and SC concentrations and patterns. However, the LREY depletion observed in SC is more marked during low flows than high flows when both colloidal fractions are more homogenous (Table 3, Fig. 2). REY concentrations in SC and CC are also impacted by hydrological conditions. They are similar in high flows (Fig. 2A and 2C) whereas low flows present more different concentrations in both rivers (Fig. 2B and 2D). The combined effect of river velocity/energy during transport, hydraulic parameters in changing hydrological conditions and aggregation/disaggregation processes could explain such differences but would require more study. Finally, the contributions of the two colloidal fractions change in the two basins, with SC dominating for the upper Alzette (Fig. 2C and 2D), whatever the hydrological conditions, whereas CC is the main contribution to the colloidal fraction in the Mess basin (Fig. 2A and 2B). Moreover, the colloidal (CC and SC) contribution to the REY concentration in the water column is more important for the Mess River than the upper Alzette River (Fig. 2). This might be a specificity related to the land use. In the Mess basin, where agricultural land dominates, soil microaggregate with sizes higher than 220 nm is the most abundant in the water column. In the upper Alzette, where urban and industrial areas are important, smaller organic colloids could dominate in comparison to coarser colloidal fractions. Overall, the available results strengthen the major influences that hydrological conditions and land uses play in controlling natural and anthropogenic REY distribution among different fractions in small contaminated rivers with important consequences for the study of REY speciation and potential ecotoxicological effects. Moreover, clay minerals may be the main carrier material to the transport of REY during flood events, especially in landscapes where soils enriched in clay material and reduced in organic matter are dominated by croplands. Finally, the aggregation/disaggregation dynamics of such particles in the river channel and their effect on REY transport deserve further investigation.

5. Conclusion

The REY positive anomalies and fractionation patterns are usually evaluated in the filterable water fractions, operationally defined as the fraction passing through the pores of 0.45 or 0.22 μm membrane filters. This approach masks the largely different REY fractionation in the dissolved and colloidal fractions, underestimates REY anomalies occurring in those fractions (notably anthropogenic Gd) and prevents a full understanding of REY geochemical cycles and fluxes in peri-urban and agricultural rivers systems.

This study confirms the necessity to consider the different fractions of the water column to evaluate the impact of anthropogenic activities on REY in polluted rivers. In order to separate suspended sediment particles and colloids from the dissolved fraction, we propose an easy-to-use methodology based on a combination between filtration and centrifuge ultrafiltration. Based on a rigorous estimation of the uncertainties, we were able to accurately separate the REY particulate, coarse and small colloidal and dissolved fractions from water collected in two contrasted peri-urban streams during both low and high flow conditions. The particulate fraction dominated the quantity of REY transported in both hydrological conditions. In low flows, the REY composition of the streams highlighted Gd, Eu and Nd anomalies related to local anthropogenic sources, with a clear dominant role of the WWTP effluent on the fractionation of the dissolved REY pattern regarding LREY and HREY. During high flows, a more natural contribution took place and dilute the anthropogenic signature, as observed for Gd, which enters the dissolved fraction as ionic species or in association with humic substances smaller than 10 kDa. We also observed processes that can be related to the river basin land use, especially for the particulate and colloidal fractions during the two contrasted hydrological conditions. Soil sealing in urbanized and industrial basins reduce the quantity of REY particulate when the erosion of soil particles enriched the suspended sediment in clays, which can be the main carrier material for REY transport on particles in such river type. The land cover also could play a role on the contributions between the coarse and small colloids, urban and industrial areas favouring the smallest fraction.

CRediT authorship contribution statement

Loïc A. Martin: Conceptualization, Methodology, Formal analysis, Data curation, Writing – original draft, Investigation, Project administration, Supervision, Validation. **Davide A.L. Vignati:** Conceptualization, Methodology, Writing – review & editing, Resources, Investigation, Project administration, Supervision, Validation. **Christophe Hissler:** Conceptualization, Methodology, Writing – review & editing, Resources, Project administration, Investigation, Supervision, Validation.

Declaration of competing interest

The authors declare that they have no known competing financial interests or personal relationships that could have appeared to influence the work reported in this paper.

Acknowledgments

This work is part of the ECOTREE project and was supported by the Luxembourg National Research Fund (FNR) and the French National Research Agency (ANR) in the framework of the FNR/INTER/ANR research programme (contract no. INTER/ANR/15/11209808/ECOTREE). We would like to thank Jean-François Iffly for the maintenance of field equipment and the accurate field data acquisition, Johanna Ziebel for her contribution in the definition of the ICP-MS analytical procedure and Lindsey Auguin, a native English speaker at LIST, for the English proofreading of the manuscript.

Appendix A. Supplementary data

All dataset presented in this study are available in the provided Supplementary Material. Supplementary data to this article can be found online at doi:https://doi.org/10.1016/j.scitotenv.2021.148207.

References

Aiken, G.R., Hsu-Kim, H., Ryan, J.N., 2011. Influence of dissolved organic matter on the environmental fate of metals, nanoparticles, and colloids. Environ. Sci. Technol. 45 (8), 3196–3201. https://doi.org/10.1021/es103992s.

Andersson, K., Dahlqvist, R., Turner, D., Stolpe, B., Larsson, T., Ingri, J., Andersson, P., 2006. Colloidal rare earth elements in a boreal river: changing sources and distributions during the spring flood. Geochim. Cosmochim. Acta 70 (13), 3261–3274. https://doi.org/10.1016/j.gca.2006.04.021.

Barber, L.B., Paschke, S.S., Battaglin, W.A., Douville, C., Fitzgerald, K.C., Keefe, S.H., Roth, D.A., Vajda, A.M., 2017. Effects of an extreme flood on trace elements in river water—from urban stream to Major River basin. Environ. Sci. Technol. 51, 10344–10356. https://doi.org/10.1021/acs.est.7b01767.

Bau, M., 1999. Scavenging of dissolved yttrium and rare earths by precipitating iron oxyhydroxide: experimental evidence for Ce oxidation, Y-ho fractionation, and lanthanide tetrad effect. Geochim. Cosmochim. Acta 63 (1), 67–77. https://doi.org/10.1016/S0016-7037(99)00014-9.

Bau, M., Dulski, P., 1996. Anthropogenic origin of positive gadolinium anomalies in river waters. Earth Planet. Sci. Lett. 143 (1–4), 245–255. https://doi.org/10.1016/0012-821X(96)00127-6.

Bau, M., Knappe, A., Dulski, P., 2006. Anthropogenic gadolinium as a micropollutant in river waters in Pennsylvania and in Lake Erie, northeastern United States. Chemie

Der Erde - Geochemistry 66 (2), 143–152. https://doi.org/10.1016/j.chemer.2006.01.002.
Bayon, G., Toucanne, S., Skonieczny, C., André, L., Bermell, S., Cheron, S., Dennielou, B., Etoubleau, J., Freslona, N., Gauchery, T., Germain, Y., Jorry, S.J., Ménot, G., Monin, L., Ponzevera, E., Rouget, M.-L., Tachikawa, K., Barrat, J.A., 2015. Rare earth elements and neodymium isotopes in world river sediments revisited. Geochim. Cosmochim. Acta 170, 17–38. https://doi.org/10.1016/j.gca.2015.08.001.
Brookins, D.G., 1989. Aqueous geochemistry of rare earth elements. Rev. Mineral. Geochem. 21, 201–225.
Buffle, J., Leppard, G.G., 1995. Characterization of aquatic colloids and macromolecules. 1. Structure and behavior of colloidal material. Environ. Sci. Technol. 29 (9), 2169–2175. https://doi.org/10.1021/es00009a004.
Coppin, F., Berger, G., Bauer, A., Castet, S., Loubet, M., 2002. Sorption of lanthanides on smectite and kaolinite. Chem. Geol. 182, 57–68.
Davranche, M., Pourret, O., Gruau, G., Dia, A., 2004. Impact of humate complexation on the adsorption of REE onto Fe oxyhydroxide. J. Colloid Interface Sci. 277 (2), 271–279. https://doi.org/10.1016/j.jcis.2004.04.007.
Davranche, M., Pourret, O., Gruau, G., Dia, A., Le Coz-Bouhnik, M., 2005. Adsorption of REE (III)-humate complexes onto MnO_2: experimental evidence for cerium anomaly and lanthanide tetrad effect suppression. Geochim. Cosmochim. Acta 69 (20), 4825–4835. https://doi.org/10.1016/j.gca.2005.06.005.
Davranche, M., Pourret, O., Gruau, G., Dia, A., Jin, D., Gaertner, D., 2008. Competitive binding of REE to humic acid and manganese oxide: impact of reaction kinetics on development of cerium anomaly and REE adsorption. Chem. Geol. 247 (1–2), 154–170. https://doi.org/10.1016/j.chemgeo.2007.10.010.
Davranche, M., Gruau, G., Dia, A., Marsac, R., Pédrot, M., Pourret, O., 2015. Biogeochemical factors affecting rare earth element distribution in shallow wetland groundwater. Aquat. Geochem. 21 (2–4), 197–215. https://doi.org/10.1007/s10498-014-9247-6.
Dia, A., Gruau, G., Olivié-Lauquet, G., Riou, C., Molénat, J., Curmi, P., 2000. The distribution of rare earth elements in groundwaters: assessing the role of source-rock composition, redox changes and colloidal particles. Geochim. Cosmochim. Acta 64 (24), 4131–4148. https://doi.org/10.1016/S0016-7037(00)00494-4.
Dupré, B., Gaillardet, J., Rousseau, D., Allègre, C.J., 1996. Major and trace elements of river-borne material: the Congo Basin. Geochim. Cosmochim. Acta 60 (8), 1301–1321. https://doi.org/10.1016/0016-7037(96)00043-9.
Elderfield, H., Upstill-Goddard, R., Sholkovitz, E.R., 1990. The rare earth elements in rivers, estuaries, and coastal seas and their significance to the composition of ocean waters. Geochim. Cosmochim. Acta 54 (4), 971–991. https://doi.org/10.1016/0016-7037(90)90432-K.
Erickson, H.P., 2009. Size and shape of protein molecules at the nanometer level determined by sedimentation, gel filtration, and electron microscopy. Biol. Proced. Online 11, 32–51. https://doi.org/10.1007/s12575-009-9008-x.
Gaillardet, J., Viers, J., Dupré, B., 2003. Trace elements in river waters. Surface and Ground Water, Weathering, and Soils: Treatise on Geochemistry. 5, pp. 225–227. https://doi.org/10.1016/B0-08-043751-6/05165-3.
Graedel, T.E., Harper, E.M., Nassar, N.T., Nuss, P., Reck, B.K., 2015. Criticality of metals and metalloids. Proc. Natl. Acad. Sci. 112, 4257–4262. https://doi.org/10.1073/pnas.1500415112.
Gruau, G., Dia, A., Olivié-Lauquet, G., Davranche, M., Pinay, G., 2004. Controls on the distribution of rare earth elements in shallow groundwaters. Water Res. 38 (16), 3576–3586. https://doi.org/10.1016/j.watres.2004.04.056.
Gustafsson, O., Gschwend, P.M., 1997. Aquatic colloids: concepts, definitions and current challanges. Limnol. Oceanogr. 42, 519–528.
Hissler, C., Stille, P., Guignard, C., Iffly, J.F., Pfister, L., 2014. Rare earth elements as hydrological tracers of anthropogenic and critical zone contributions: a case study at the Alzette River basin scale. Procedia Earth and Planetary Science 10, 349–352. https://doi.org/10.1016/j.proeps.2014.08.036.
Hissler, C., Hostache, R., Iffly, J.F., Pfister, L., Stille, P., 2015a. Anthropogenic rare earth element fluxes into floodplains: coupling between geochemical monitoring and hydrodynamic sediment transport modelling. Compt. Rendus Geosci. 347, 294–303. https://doi.org/10.1016/j.crte.2015.01.003.
Hissler, C., Stille, P., Juilleret, J., Iffly, J.F., Perrone, T., Morvan, G., 2015b. Elucidating the formation of terra fuscas using Sr-Nd-Pb isotopes and rare earth elements. Appl. Geochem. 54, 85–99. https://doi.org/10.1016/j.apgeochem.2015.01.011.
Hissler, C., Stille, P., Iffly, J.F., Guignard, C., Chabaux, F., Pfister, L., 2016. Origin and dynamics of rare earth elements during flood events in contaminated river basins: Sr-Nd-Pb isotopic evidence. Environ. Sci. Technol. 50 (9), 4624–4631. https://doi.org/10.1021/acs.est.5b03660.
Hostache, R., Hissler, C., Matgen, P., Guignard, C., Bates, P., 2014. Modelling suspended-sediment propagation and related heavy metal contamination in floodplains: a parameter sensitivity analysis. Hydrol. Earth Syst. Sci. 18 (9), 3539–3551. https://doi.org/10.5194/hess-18-3539-2014.
Ingrao, N.J., Hammouda, T., Boyet, M., Gaborieau, M., Moine, B.N., Vlastelic, I., Vlastelic, I., Bouhfid, M.A., Devidal, J.-L., Mathon, O., Testemale, D., Hazemann, J.-L., Proux, O., 2019. Rare earth element partitioning between sulphides and melt: evidence for Yb^{2+} and Sm^{2+} in EH chondrites. Geochim. Cosmochim. Acta 265, 182–197. https://doi.org/10.1016/j.gca.2019.08.036.
Johnsen, E., Kristian, O., Vehus, T., Roberg-larsen, H., Bogoeva, V., Ademi, O., Hildahl, J., Lundanes, E., Ray, S., 2016. A critical evaluation of Amicon ultra centrifugal filters for separating proteins, drugs and nanoparticles in biosamples. J. Pharm. Biomed. Anal. 120, 106–111. https://doi.org/10.1016/j.jpba.2015.12.010.
Klaver, G., Verheul, M., Bakker, I., Petelet-Giraud, E., Négrel, P., 2014. Anthropogenic rare earth element in rivers: gadolinium and lanthanum. Partitioning between the dissolved and particulate phases in the Rhine River and spatial propagation through the Rhine-Meuse Delta (the Netherlands). Appl. Geochem. 47, 186–197. https://doi.org/10.1016/j.apgeochem.2014.05.020.
Knobloch, V., Zimmermann, T., Gößling-Reisemann, S., 2018. From criticality to vulnerability of resource supply: the case of the automobile industry. Resour. Conserv. Recycl. 138, 272–282. https://doi.org/10.1016/j.resconrec.2018.05.027.
Kottelat, R., Vignati, D.A.L., Chanudet, V., Dominik, J., 2008. Comparison of small- and large-scale ultrafiltration systems for organic carbon and metals in freshwater at low concentration factor. Water Air Soil Pollut. 187, 343–351. https://doi.org/10.1007/s11270-007-9504-z.
Kulaksiz, S., Bau, M., 2007. Contrasting behaviour of anthropogenic gadolinium and natural rare earth elements in estuaries and the gadolinium input into the North Sea. Earth Planet. Sci. Lett. 260, 361–371. https://doi.org/10.1016/j.epsl.2007.06.016.
Kulaksiz, S., Bau, M., 2011a. Rare earth elements in the Rhine River, Germany: first case of anthropogenic lanthanum as a dissolved microcontaminant in the hydrosphere. Environ. Int. 37 (5), 973–979. https://doi.org/10.1016/j.envint.2011.02.018.
Kulaksiz, S., Bau, M., 2011b. Anthropogenic gadolinium as a microcontaminant in tap water used as drinking water in urban areas and megacities. Appl. Geochem. 26 (11), 1877–1885. https://doi.org/10.1016/j.apgeochem.2011.06.011.
Kulaksiz, S., Bau, M., 2013. Anthropogenic dissolved and colloid/nanoparticle-bound samarium, lanthanum and gadolinium in the Rhine River and the impending destruction of the natural rare earth element distribution in rivers. Earth Planet. Sci. Lett. 362, 43–50. https://doi.org/10.1016/j.epsl.2012.11.033.
Larsson, J., Gustafsson, Ö., Ingri, J., 2002. Evaluation and optimization of two complementary cross-flow ultrafiltration systems toward isolation of coastal surface water. Environ. Sci. Technol. 36, 2236–2241. https://doi.org/10.1021/es010325v.
Lead, J.R., Wilkinson, K.J., 2006. Aquatic colloids and nanoparticles: current knowledge and future trends. Environ. Chem. 3, 159–171. https://doi.org/10.1071/EN06025.
Liu, W., Etschmann, B., Migdisov, A., Boukhalfa, H., Testemale, D., Müller, H., Hazemann, J.-L., Brugger, J., 2017. Revisiting the hydrothermal geochemistry of europium(II/III) in light of new in-situ XAS spectroscopy results. Chem. Geol. 459, 61–74. https://doi.org/10.1016/j.chemgeo.2017.04.005.
Louis, P., Messaoudene, A., Jrad, H., Abdoul-Hamid, B.A., Vignati, D.A.L., Pons, M.-N., 2020. Understanding rare earth elements concentrations, anomalies and fluxes at the river basin scale: the Moselle River (France) as a case study. Sci. Total Environ. 742, 140619. https://doi.org/10.1016/j.scitotenv.2020.140619.
Maleke, M., Valverde, A., Gomez-Arias, A., Cason, E.D., Vermeulen, J.G., Coetsee-Hugo, L., Swart, E., van Heerden, E., Castillo, J., 2019. Anaerobic reduction of europium by a Clostridium strain as a strategy for rare earth biorecovery. Sci. Rep. 9 (1), 1–11. https://doi.org/10.1038/s41598-019-50179-z.
McLennan, S.M., 1989. Rare earth elements in sedimentary rocks: influence of provenance and sedimentary processes. Rev. Mineral. Geochem. 21, 169–200.
Merschel, G., Bau, M., Baldewein, L., Dantas, E.L., Walde, D., Bühn, B., 2015. Tracing and tracking wastewater-derived substances in freshwater lakes and reservoirs: anthropogenic gadolinium and geogenic REEs in Lake Paranoá, Brasilia. Compt. Rendus Geosci. 347 (5–6), 284–293. https://doi.org/10.1016/j.crte.2015.01.004.
Merschel, G., Bau, M., Dantas, E.L., 2017. Contrasting impact of organic and inorganic nanoparticles and colloids on the behavior of particle-reactive elements in tropical estuaries: an experimental study. Geochim. Cosmochim. Acta 197, 1–13. https://doi.org/10.1016/j.gca.2016.09.041.
Miller, J.N., Miller, J.C., 2010. Statistics and Chemometrics for Analytical Chemistry. 6th ed. Pearson Education Limited, Horlow, England, pp. 110–153.
Möller, P., Dulski, P., 2010. Transmetallation of Gd-DTPA by Cu, Y and lanthanides and its impact on the hydrosphere. Appl. Geochem. 25 (1), 48–59. https://doi.org/10.1016/j.apgeochem.2009.09.027.
Nozaki, Y., Lerche, D., Alibo, D.S., Tsutsumi, M., 2000. Dissolved indium and rare earth elements in three Japanese rivers and Tokyo Bay: evidence for anthropogenic Gd and In. Geochim. Cosmochim. Acta 64, 3975–3982. https://doi.org/10.1016/S0016-7037(00)00472-5.
Ohta, A., Kawabe, I., 2001. REE(III) adsorption onto Mn dioxide (δ-MnO_2) and Fe oxyhydroxide: Ce(III) oxidation by δ-MnO_2. Geochim. Cosmochim. Acta 65 (5), 695–703.
Parant, M., Perrat, E., Wagner, P., Rosin, C., Py, J.-S., Cossu-Leguille, C., 2018. Variations of anthropogenic gadolinium in rivers close to waste water treatment plant discharges. Environ. Sci. Pollut. Res. 25, 36207–36222. https://doi.org/10.1007/s11356-018-3489-6.
Pédrot, M., Dia, A., Davranche, M., Bouhnik-Le Coz, M., Henin, O., Gruau, G., 2008. Insights into colloid-mediated trace element release at the soil/water interface. J. Colloid Interface Sci. 325 (1), 187–197. https://doi.org/10.1016/j.jcis.2008.05.019.
Pédrot, M., Dia, A., Davranche, M., Gruau, G., 2015. Upper soil horizons control the rare earth element patterns in shallow groundwater. Geoderma 239, 84–96. https://doi.org/10.1016/j.geoderma.2014.09.023.
Pfister, L., Martínez-Carreras, N., Hissler, C., Klaus, J., Carrer, G.E., Stewart, M.K., McDonnell, J.J., 2017. Bedrock geology controls on catchment storage, mixing, and release: a comparative analysis of 16 nested catchments. Hydrol. Process. 31 (10), 1828–1845. https://doi.org/10.1002/hyp.11134.
Pokrovsky, O.S., Schott, J., Dupré, B., 2006. Trace element fractionation and transport in boreal rivers and soil porewaters of permafrost-dominated basaltic terrain in Central Siberia. Geochim. Cosmochim. Acta 70 (13), 3239–3260. https://doi.org/10.1016/j.gca.2006.04.008.
Pourret, O., Davranche, M., Gruau, G., Dia, A., 2007a. Competition between humic acid and carbonates for rare earth elements complexation. J. Colloid Interface Sci. 305 (1), 25–31. https://doi.org/10.1016/j.jcis.2006.09.020.
Pourret, O., Davranche, M., Gruau, G., Dia, A., 2007b. Organic complexation of rare earth elements in natural waters: Evaluating model calculations from ultrafiltration data. Geochim. Cosmochim. Acta 71 (11), 2718–2735. https://doi.org/10.1016/j.gca.2007.04.001.

Pourret, O., Davranche, M., Gruau, G., Dia, A., 2007c. Rare earth elements complexation with humic acid. Chem. Geol. 243 (1–2), 128–141. https://doi.org/10.1016/j.chemgeo.2007.05.018.

Pourret, O., Gruau, G., Dia, A., Davranche, M., Molénat, J., 2010. Colloidal control on the distribution of rare earth elements in shallow groundwaters. Aquat. Geochem. 16, 31–59. https://doi.org/10.1007/s10498-009-9069-0.

Sholkovitz, E.R., 1992. Chemical evolution of rare earth elements: fractionation between colloidal and solution phases of filtered river water. Earth Planet. Sci. Lett. 114, 77–84.

Smirnova, E.V., Mysovskaya, I.N., Lozhkin, V.I., Sandimirova, G.P., Pakhomova, N.N., Smagunova, A.A., 2006. Spectral interferences from polyatomic barium ions in inductively coupled plasma mas spectrometry. J. Appl. Spectrosc. 73 (6), 813–818.

Steinmann, P., Billen, T., Loizeau, J.I., Dominik, J., 1999. Beryllium-7 as a tracer to study mechanisms and rates of metal scavenging from lake surface waters. Geochim. Cosmochim. Acta 63 (11-12), 1621–1633.

Stolpe, B., Guo, L., Shiller, A.M., Aiken, G.R., 2012. Abundance, size distributions and trace-element binding of organic and iron-rich nanocolloids in Alaskan rivers, as revealed by field-flow fractionation and ICP-MS. Geochim. Cosmochim. Acta 105, 221–239. https://doi.org/10.1016/j.gca.2012.11.018.

Tang, J., Johannesson, K.H., 2003. Speciation of rare earth elements in natural terrestrial waters: assessing the role of dissolved organic matter from the modeling approach. Geochim. Cosmochim. Acta 67 (13), 2321–2339. https://doi.org/10.1016/S0016-7037(02)01413-8.

Tepe, N., Romero, M., Bau, M., 2014. High-technology metals as emerging contaminants: strong increase of anthropogenic gadolinium levels in tap water of Berlin, Germany, from 2009 to 2012. Appl. Geochem. 45, 191–197. https://doi.org/10.1016/j.apgeochem.2014.04.006.

Town, R.M., Filella, M., 2002. Size fractionation of trace metal species in freshwaters: implications for understanding their behaviour and fate: metal size fractionation and speciation. Rev. Environ. Sci. Biotechnol. 1 (4), 277–297. https://doi.org/10.1023/A:1023229825984.

Verplanck, P.L., Furlong, E.T., Gray, J.L., Phillips, P.J., Wolf, R.E., Esposito, K., 2010. Evaluating the behavior of gadolinium and other rare earth elements through large metropolitan sewage treatment plants. Environ. Sci. Technol. 44 (10), 3876–3882. https://doi.org/10.1021/es903888t.

Vignati, D., Dominik, J., 2003. The role of coarse colloids as a carrier phase for trace metals in riverine systems. Aquat. Sci. 65 (2), 129–142. https://doi.org/10.1007/s00027-003-0640-2.

Wrede, S., Fenicia, F., Martínez-carreras, N., Juilleret, J., Hissler, C., Krein, A., Savenije, H.H.G., Uhlenbrook, S., Kavetski, D., Laurent, P., 2015. Towards more systematic perceptual model development: a case study using 3 Luxembourgish catchments. Hydrol. Process. 29, 2731–2750. https://doi.org/10.1002/hyp.10393.

Yang, M., Liang, X., Ma, L., Huang, J., He, H., Zhu, J., 2019. Adsorption of REEs on kaolinite and halloysite: a link to the REE distribution on clays in the weathering crust of granite. Chem. Geol. 525(June, 210–217. https://doi.org/10.1016/j.chemgeo.2019.07.024.

Yeghicheyan, D., Aubert, D., Bouhnik-Le Coz, M., Chmeleff, J., Delpoux, S., Djouraev, I., Granier, G., Lacan, F., Piro, J.-L., Rousseau, T., Cloquet, C., Marquet, A., Menniti, C., Pradoux, C., Freydier, R., Viera da Silva-Filho, E., Suchorski, K., 2019. A new Interlaboratory characterisation of silicon, rare earth elements and twenty-two other trace element concentrations in the natural river water certified reference material SLRS-6 (NRC-CNRC). Geostand. Geoanal. Res. 43 (3), 475–496. https://doi.org/10.1111/ggr.12268.

Zhang, S., Ding, Y., Liu, B., Chang, C.-c, 2017. Supply and demand of some critical metals and present status of their recycling in WEEE. Waste Manag. 65, 113–127. https://doi.org/10.1016/j.wasman.2017.04.003.